Numerical Analysis of Mixed Convective Peristaltic Flow in a Vertical Channel in Presence of Heat Generation without using Lubrication Theory

B. Ahmed[†], T. Javed, A. H. Hamid and M. Sajid

Department of Mathematics and Statistics, International Islamic University Islamabad Pakistan

†*Corresponding Author Email: bilalmaths7@yahoo.com*

ABSTRACT

In this paper, heat transfer analysis of peristaltic mixed convection flow through a vertical channel is presented in addition, effects of heat generation are also investigated. The mathematical model is represented by the system of non-linear partial differential equations. The analysis is made in the presence of non-zero wave and Reynolds numbers. The results of the long wavelength assumption in a creeping flow can be deduced. These results thus predict new features in the peristaltic transport in the absence of the approximation of long wave length and low Reynolds number. The moderate finite elements based technique has been used to compute the highly accurate solution of the governing problem. To ensure the accuracy of the computed solution, the results obtained are validated against the available results in the literature and found good agreement. The obtained result are presented through graphs and the influence of involved pertinent parameters is analyzed.

Keywords: Mixed convection; Peristaltic flow; Heat generation; Numerical analysis; Non-zero Reynolds number.

1. INTRODUCTION

Importance of fluid mechanics in industrial and technological applications attracted the attentions of scientists, engineers and mathematician to study the fluid behavior in different geometries. The manufacturing processes like glass fiber production, sheets production, hot rolling, continuous casting, extrusion process, coating and paper production etc. involves fluid mechanism. Furthermore, advancements in fluid mechanics also assists in developing of heating and ventilating systems for industrial and domestic purposes. The designing of pipeline systems also requires the basic understanding of fluid flows. In the field of medical science, the importance of fluid mechanics increases significantly as it is useful in designing of blood substitutes, artificial hearts, heart-lung machines, breathing aids and other such type of devices, which all obeys the basic principles of fluid mechanics. The flow generated by sinusoidal motion of the boundary of a vessel is known as peristaltic flow. Peristalsis is a common mechanism found in physiological and industrial processes. The most common examples of physiological flows involving peristalsis include flow of urine from kidney to the bladder, flow of chyme in small intestine, blood flow through capillaries, spermatic fluid transport in female reproductive tract etc. The transport in corrosive fluid in the nuclear industry, diabetes pumps and pharmacological delivery systems involve peristaltic mechanism.

In the literature different aspects of the peristaltic flow are discussed analytically and experimentally. The presence of non-linearity due to the finite Reynolds number makes theoretical investigations more difficult. Many analytical studies involves perturbation techniques through which an explicit form of the solution is obtained that helps in understanding physical effects of the parameters. Peristaltic mechanism first studied by Latham (1966) both theoretically and experimentally. This work open new venues of research to understand peristaltic mechanism in the presence of new aspects. A number of articles (Weinberg *et al*. 1971; Lew *et al*. 1971; Ali *et al*. 2010; Manton 1975; Jaffrin 1973; Dharmrndra Tripathi 2013; Rao and Usha 1995; Narahari and Sreenadh 2010; Shapiro 1967) addressing the peristaltic phenomenon for different type of geometries under the assumption of long wavelength and low Reynolds number, small amplitude ratio and wave number are available. The lubrication theory was used by Shapiro *et al*. (1969) to investigate the peristaltic phenomenon in a two dimensional channel using a wave frame of

reference. On the other hand, Fung and Yih (1968) used fixed frame of reference for investigating peristaltic flow without using lubrication approach. The non-linear terms get vanished through the approach by Shapiro *et al.* (1969) and problem become simpler on comparison to Fung and Yih (1968) approach. In this approach effects of Reynolds number and wave number (rates of characteristic length of the channel/tube to the wave length of the peristaltic wave) on various flow characteristics cannot be investigated. Due to simplicity of the approach, this theory is used widely to study the peristaltic flow of Newtonian and non-Newtonian fluid in number of scenarios. Jaffrin (1973) discussed the perturbation solution of two dimensional peristaltic flow in a channel. Zien and Ostrach (1970) also discussed the peristaltic mechanism. Takabatake (1989) and Ayukawa (1990) employed the finite difference method to numerically simulate two-dimensional peristaltic flow in a channel for moderate values of the Reynolds numbers and wave numbers. They showed that the perturbation solution of Jaffrin (1973) but Zien and Ostrach (1970) presented the result in a narrow range and in accordance of Reynolds number the reflux phenomenon does not cause the change the whole situation in the flow. The application of immersed boundary technique to simulate the transport solid particle in a two-dimensional channel by peristalsis was initiated by Fouci (1992). Mekheimer (2008) discussed the magnetohydrodynamic effect in the natural limitation of peristaltic phenomenon, which is not valid for moderate values of both Reynolds number and wave number. Considerable investigation for peristaltic transport pumping problem are formulated (Ekstein 1970; Hung and Brown 1975.

Sajid *et al.* (2015) investigated the mixed convection behavior of an Oldroyd-B fluid. Vajravelua *et al.* (2007) studied heat transfer analysis in peristaltic flow through a vertical porous annulus under long wavelength approximation. A note on peristaltic transport in an asymmetric channel with heat transfer is presented by Srinivas *et al.* (2008). In axisymmetric, channel mixed convective heat and mass transfer analysis were presented by Srinivas *et al.* (2011). In both studies, they apply the long wavelength approximation. Mixed convection in peristalsis transport model nowadays gain deep interest by the researchers, so the articles related to peristaltic motion in different physical situation of mixed convection are found in literature (Sayed et. al 2015; Tanveer *et al.* 2017; Hayat *et al.* 2017; Sucharitha 2017). K. Ramesh (2016) recently studied the peristaltic flow in the presence of slip and convective conditions through porous medium. He obtained simplification using the lubrication theory. Recently, Hamid *et al.* (2017) studied the peristaltic flow numerically for two dimensional non-Newtonian fluid without employing the lubrication theory.

The aim of this article is to analyze the mixed convection in peristaltic flow in a vertical channel in the presence of heat generation and streamline curvature effects by dropping the assumption of long

wavelength and low Reynolds number. First, we develop the problem in wave frame by using formulation of stream function and vorticity. The pressure is eliminated by cross differentiation and discussed by explicit expression given in latter part. The numerical solution of the problem is computed with the help of finite element method which give us the liberty to set high values of Reynolds number and other suitable values of the involved parameters. The result are discussed in the last part with different versions of presentation.

2. PROBLEM DEVELOPMENT

Consider the motion of Newtonian fluid through a vertical channel having inner width size $2d$. The flow is assumed in such a way that propagation of waves is along the *x*-axis with velocity *c* and *y* is along normal to the channel. The peristaltic wall of channel are assumed at some amount of temperature T_1 and obeys the sinusoidal wave shape represented by

$$H(X,t) = a - b\cos\left\{\frac{2\pi(X - ct)}{\lambda}\right\}, \qquad (1)$$

where *b* is wave amplitude, λ represents wave length and *h* is the symbol for mean distance of the wall from the central axis as shown in Fig. 1. The coordinates of velocity, pressure and temperature in fixed and moving frame of reference are related by set of following expression

$$
\begin{aligned}
x^* &= X - ct, & y^* &= Y, & u^* &= U - c, \\
v^* &= V, & p &= p^*, & T^* &= T_1,
\end{aligned}
\qquad (2)
$$

where (u^*, v^*) and (U, V) represent the components of velocity vectors in moving frame of reference and fixed frame of reference respectively.
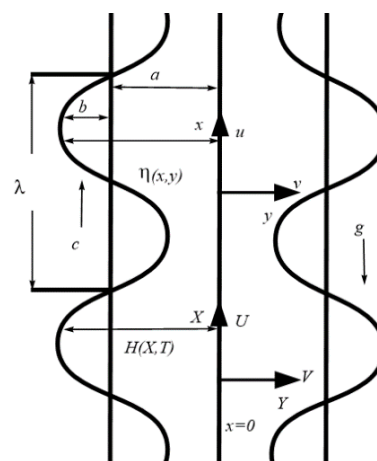
Fig. 1. The geometry of considered two-dimensional peristaltic channel.

In fixed frame of reference, the continuity, momentum and energy equations for the assumed problem are

$$\frac{\partial U}{\partial X} + \frac{\partial V}{\partial Y} = 0, \tag{3}$$

$$\rho\left(\frac{\partial U}{\partial t} + U\frac{\partial U}{\partial X} + V\frac{\partial U}{\partial Y}\right) = -\frac{\partial p}{\partial X}$$
$$+ \mu\left(\frac{\partial^2 U}{\partial X^2} + \frac{\partial^2 U}{\partial Y^2}\right) + \rho g \beta_T (T - T_0), \tag{4}$$

$$\rho\left(\frac{\partial V}{\partial t} + U\frac{\partial V}{\partial X} + V\frac{\partial V}{\partial Y}\right) = -\frac{\partial p}{\partial Y}$$
$$+ \mu\left(\frac{\partial^2 V}{\partial X^2} + \frac{\partial^2 V}{\partial Y^2}\right), \tag{5}$$

$$\rho c_p\left(\frac{\partial U}{\partial t} + U\frac{\partial T}{\partial X} + V\frac{\partial T}{\partial Y}\right) =$$
$$\kappa^*\left(\frac{\partial^2 T}{\partial X^2} + \frac{\partial^2 T}{\partial Y^2}\right) + Q_0. \tag{6}$$

in which μ is the viscosity ρ is the density, g is the acceleration caused by gravity, β_T is thermal expansion coefficient, c_p is specific heat at constant pressure, κ^* is the thermal conductivity and Q_0 represents constant heat generation with in the flow domain.

The boundary conditions of the problem are

$$V = 0, \quad \frac{\partial U}{\partial Y} = 0, \quad \frac{\partial T}{\partial Y} = 0 \ \ at \ Y = 0, \tag{7}$$

$$U = 0, \quad V = \frac{\partial H}{\partial T}, \quad T = T_1 \ \ at \ Y = H. \tag{8}$$

Equations that governs the flow in wave frame are as follows

$$\frac{\partial u^*}{\partial x^*} + \frac{\partial v^*}{\partial y^*} = 0, \tag{9}$$

$$\rho\left(u^*\frac{\partial u^*}{\partial x^*} + v^*\frac{\partial u^*}{\partial y^*}\right) = -\frac{\partial p^*}{\partial x^*}$$
$$+ \mu\left(\frac{\partial^2 u^*}{\partial x^{*2}} + \frac{\partial^2 u^*}{\partial y^{*2}}\right) + \rho g \beta_T (T^* - T_0), \tag{10}$$

$$\rho\left(u^*\frac{\partial v^*}{\partial x^*} + v^*\frac{\partial v^*}{\partial y^*}\right) = -\frac{\partial p^*}{\partial y^*}$$
$$+ \mu\left(\frac{\partial^2 v^*}{\partial x^{*2}} + \frac{\partial^2 v^*}{\partial y^{*2}}\right), \tag{11}$$

$$\rho c_p\left(u^*\frac{\partial T^*}{\partial x^*} + v^*\frac{\partial T^*}{\partial y^*}\right) = \kappa^*\left(\frac{\partial^2 T^*}{\partial x^{*2}} + \frac{\partial^2 T^*}{\partial y^{*2}}\right) + Q_0 \tag{12}$$

The configuration of the peristaltic wall can be written as

$$\eta(x^*) = a - b\cos\left(\frac{2\pi x^*}{\lambda}\right), \tag{13}$$

and the no slip and the symmetry condition on the planes $y^* = 0$ and $y^* = \eta(x^*)$ respectively can be expressed as follows

$$v^* = 0, \ \frac{\partial u^*}{\partial y^*} = 0, \ \frac{\partial T^*}{\partial y^*} = 0 \ at \ y^* = 0, \tag{14}$$

$$u^* = c, \ v^* = \frac{2\pi b}{\lambda}\sin\left(\frac{2\pi x^*}{\lambda}\right),$$
$$T^* = T_1 \ \ at \ y^* = \eta(x^*). \tag{15}$$

As both planes $y^* = 0$ and $y^* = \eta(x^*)$, present streamline and flow rate q^* is constant in cross section of the channel in wave frame, therefore

$$\psi^* = 0 \ on \ y^* = 0,$$
$$\psi^* = q^* \ on \ y = \eta\ (x^*), \tag{16}$$

where $q^* = Q^* - ch$ is the relation between flow rate in the wave frame of refrence and the time mean flow in the laboratory frame Q^*.

Defining new variables

$$x = \frac{x^*}{\lambda}, \ y = \frac{y^*}{a}, \ u = \frac{u^*}{c}, \ v = \frac{v^*}{c}, \ \alpha = \frac{a}{\lambda},$$

$$h = \frac{h(x^*)}{a}, \quad p = \frac{a^2}{\lambda\mu c}p^*(x^*), \quad \eta = \frac{\eta^*}{h},$$

$$\psi = \frac{\psi^*}{ca}, \ \omega = \frac{\omega^*}{c/a}, \ q = \frac{q^*}{ch}, \ \theta = \frac{T^* - T_0}{T_1 - T_0},$$

$$\mathrm{Re} = \frac{ca}{v}\alpha, \ Gr = \frac{\rho g a \beta(T_1 - T_0)}{\mu c},$$

$$\mathrm{Pr} = \frac{\mu c}{k^*}, \ \beta = \frac{Q_0 a^2}{\kappa^*(T_1 - T_0)}.$$

Eqs., (9) – (12) takes the form

$$\alpha^2\frac{\partial^2\psi}{\partial x^2} + \frac{\partial^2\psi}{\partial y^2} = -\omega, \tag{17}$$

$$\mathrm{Re}\left(\frac{\partial\psi}{\partial y}\frac{\partial\omega}{\partial x} - \frac{\partial\psi}{\partial x}\frac{\partial\omega}{\partial y}\right) = \nabla^2\omega + Gr\frac{\partial\theta}{\partial y}, \tag{18}$$

$$\mathrm{Re}\,\mathrm{Pr}\left(\frac{\partial\psi}{\partial y}\frac{\partial\theta}{\partial x} - \frac{\partial\psi}{\partial x}\frac{\partial\theta}{\partial y}\right) = \nabla^2\theta + \beta, \tag{19}$$

where Re is Reynolds number, α is wave number, Gr is Grashof number, β is heat generation parameter and Pr is Prandtl number. The boundary conditions in terms of $\psi(x, y)$ are as follow

$$\psi = 0, \ \frac{\partial^2 \psi}{\partial y^2} = 0,$$

$$\frac{\partial \psi}{\partial x} = 0, \ \frac{\partial \theta}{\partial x} = 0 \qquad \text{at } y = 0, \tag{20}$$

$$\psi = q, \ \frac{\partial \psi}{\partial y} = -1, \ \theta = 1,$$

$$\frac{\partial \psi}{\partial x} = 2\pi\phi\sin 2\pi x \qquad \text{at } y = \eta(x),$$

where

$$u = \frac{\partial \psi}{\partial y}, \qquad \nabla^2 = \alpha^2 \frac{\partial^2}{\partial x^2} + \frac{\partial^2}{\partial y^2},$$

$$v = -\alpha\frac{\partial \psi}{\partial x} \text{ and } \omega = \alpha\frac{\partial v}{\partial x} - \frac{\partial u}{\partial y}. \tag{21}$$

3. NUMERICAL ANALYSIS

In the previous sections the obtained equations are valid for non-zero Reynolds and wave numbers and cannot be transferred to ordinary differential equations. Finite element method has been preferred in the current investigation due to its several advantages over other methods generally used to solve numerical problems. The foremost advantage of finite element method is that it works with non-uniform mesh which results in more accurate numerical approximation particular when you are dealing with complex geometries and irregular boundary conditions. Providing the user liberty to choose the shape functions and types of elements according to the problem. This approach returns more accurate solutions with less computational cost. To deal with the partial differential equations finite element method of Gelerikin's approach is applied to solve Eqs. (17)-(19) subject to the boundary conditions (20) in a finite region of L number of waves in a wave frame having two end sections with one fixed and other moving boundary. Because of the continuity of the flow we consider single wave at a time and then follow the next and so on. In all the cases, the computed results are highly convergent and satisfy the tolerance of $\varepsilon_\psi = 10^{-14}, \varepsilon_\omega = 10^{-14}$ and $\varepsilon_T = 10^{-13}$. The numerical computations are made by using non-uniform meshing of quadratic elements with the help of pdetool available in MATLAB. The stream function, vorticity as well as temperature functions are approximated by

$$\psi = \sum_{k=1}^{n} N_k\psi_k, \ \omega = \sum_{k=1}^{n} N_k\omega_k, \ \theta = \sum_{k=1}^{n} N_k\theta_k, \tag{22}$$

in which ψ_k, ω_k and θ_k are element nodal approximation of ψ, ω and θ. Then Galerkin finite element is endorsed to governing Eqs. (17)-(19) as follows

$$\int_\Omega w_1\left(\alpha^2 \frac{\partial^2 \psi}{\partial x^2} + \frac{\partial^2 \psi}{\partial y^2} + \omega\right) d\Omega = 0, \tag{23}$$

$$\int_\Omega w_2 \left[\begin{array}{c} \text{Re}\left(\dfrac{\partial \psi}{\partial y}\dfrac{\partial \omega}{\partial x} - \dfrac{\partial \psi}{\partial x}\dfrac{\partial \omega}{\partial y}\right) \\ -\left(\alpha^2 \dfrac{\partial^2 \omega}{\partial x^2} + \dfrac{\partial^2 \omega}{\partial y^2}\right) - Gr\dfrac{\partial \theta}{\partial y} \end{array} \right] d\Omega = 0, \tag{24}$$

$$\int_\Omega w_3 \left[\begin{array}{c} \text{RePr}\left(\dfrac{\partial \psi}{\partial y}\dfrac{\partial \theta}{\partial x} - \dfrac{\partial \psi}{\partial x}\dfrac{\partial \theta}{\partial y}\right) \\ -\left(\alpha^2 \dfrac{\partial^2 \theta}{\partial x^2} + \dfrac{\partial^2 \theta}{\partial y^2}\right) - \beta \end{array} \right] d\Omega = 0, \tag{25}$$

where W_1, W_2 and W_3 are weight functions. After simplifying Eqs. (23)-(25), we obtain

$$\int_\Omega \left(\alpha^2 \frac{\partial w_1}{\partial x}\frac{\partial \psi}{\partial x} + \frac{\partial w_1}{\partial y}\frac{\partial \psi}{\partial y}\right) d\Omega$$
$$- \int_\Omega w_1\omega d\Omega = \int_\Gamma w_1 \frac{\partial \psi}{\partial n}d\Gamma, \tag{26}$$

$$\int_\Omega \text{Re}\, w_2\left(\frac{\partial \psi}{\partial y}\frac{\partial \omega}{\partial x} - \frac{\partial \psi}{\partial x}\frac{\partial \omega}{\partial y}\right) d\Omega$$
$$+ \int_\Omega \left(\alpha^2 \frac{\partial w_2}{\partial x}\frac{\partial \omega}{\partial x} + \frac{\partial w_2}{\partial y}\frac{\partial \omega}{\partial y}\right) d\Omega \tag{27}$$
$$- Gr\int_\Omega w_2 \frac{\partial \theta}{\partial y}d\Omega = \int_\Gamma w_2 \frac{\partial \omega}{\partial n}d\Gamma,$$

$$\int_\Omega \text{RePr}\, w_3\left(\frac{\partial \psi}{\partial y}\frac{\partial \theta}{\partial x} - \frac{\partial \psi}{\partial x}\frac{\partial \theta}{\partial y}\right) d\Omega$$
$$+ \int_\Omega \left(\alpha^2 \frac{\partial w_3}{\partial x}\frac{\partial \theta}{\partial x} + \frac{\partial w_3}{\partial y}\frac{\partial \theta}{\partial y}\right) d\Omega \tag{28}$$
$$- \int_\Omega w_3\beta d\Omega = \int_\Gamma w_3 \frac{\partial \theta}{\partial n}d\Gamma.$$

By considering the discretized domain, we plugin Eq. (22) in (26)-(28) to get

$$-\sum_i B_{ki}^e\omega_i + \sum_i A_{ki}^e\psi_i = S_n^{k^e}, \tag{29}$$

$$\sum_i A_{ki}^e\omega_i + \text{Re}\sum_i C_{kij}^e\psi_i\omega_i - Gr\sum_i B1_{ki}^e\theta_i = S_n^{k^e}, \tag{30}$$

$$\sum_i A_{ki}^e\theta_i + \text{RePr}\sum_i C_{kij}^e\psi_i\theta_i = S_n^{k^e} + \beta S^{k^e}, \tag{31}$$

where

$$A_{ki}^e = \int_{\Omega^e} \left(\alpha^2 \frac{\partial N_k}{\partial x}\frac{\partial N_i}{\partial x} + \frac{\partial N_k}{\partial y}\frac{\partial N_i}{\partial y}\right) d\Omega, \tag{32}$$

$$B_{ki}^e = \int_{\Omega^e} N_k N_i d\Omega, \ B1_{ki}^e = \int_{\Omega^e} N_k \frac{\partial N_i}{\partial y}d\Omega,$$

$$C_{kij}^e = \int_{\Omega^e} N_k\left(\frac{\partial N_i}{\partial y}\frac{\partial N_j}{\partial x} - \frac{\partial N_j}{\partial x}\frac{\partial N_i}{\partial y}\right) d\Omega,$$

$$S^{k^e} = \int_\Gamma N_k d\Gamma \text{ and } S_n^{k^e} = \int_\Gamma N_k \overline{S}_k d\Gamma.$$

The global system in form of matrix is defined as

$$KA = F, \tag{33}$$

where

$$K_{ij} = \begin{bmatrix} -B_{ki}^e & A_{ki}^e & 0 \\ A_{ki}^e & \text{Re}\,C_{kij}^e \omega_i & -GrB1_{ki}^e \\ 0 & \text{Re}\,\text{Pr}\,C_{kij}^e \theta_i & A_{ki}^e \end{bmatrix}, \tag{34}$$

$$A_k = \begin{bmatrix} \omega_k \\ \psi_k \\ \theta_k \end{bmatrix}, \quad F = \begin{bmatrix} S_n^{k^e} \\ 0 \\ S_n^{k^e} + \beta S^{k^e} \end{bmatrix}.$$

The obtained non-linear equations are then solved by using famous Newton-Raphson method. The solution process is iterated unless the error between two consecutive iterations is become not less than 10^{-14}.

4. ANALYSIS OF THE PRESSURE

Since the flow is caused by the infinite train of sinusoidal waves of same period, therefore evaluate the pressure at the central part of considered domain which covers the region of one wave length, The dimensionless form of the expressions for pressure gradient is obtained from two dimensional form of Naiver-Stokes equations for steady flow as

$$\frac{\partial P}{\partial x} = \text{Re}\left(\frac{\partial^2 \psi}{\partial y^2} \frac{\partial \psi}{\partial x} - \frac{\partial^2 \psi}{\partial x \partial y} \frac{\partial \psi}{\partial y} \right) - \frac{\partial \omega}{\partial y} + Gr\theta. \tag{35}$$

$$\frac{\partial P}{\partial y} = \text{Re}\,\alpha^2 \left(\frac{\partial^2 \psi}{\partial x^2} \frac{\partial \psi}{\partial y} - \frac{\partial^2 \psi}{\partial x \partial y} \frac{\partial \psi}{\partial x} \right) - \alpha \frac{\partial \omega}{\partial x}. \tag{36}$$

The pressure-rise per wave length in the wave frame are defined as

$$\Delta p_\lambda = \int_0^\lambda \frac{dp}{dx} dx. \tag{37}$$

5. RESULTS AND DISCUSSION

In this section, we analyzed the results of the modelled problem in terms of velocity distribution, heat characteristics, trapping phenomenon and rise in pressure against different involved flow parameters.

5.1 Velocity Field and Temperature Characteristics

A comparison of the obtained numerical results with the analytical results of Srinivas *et al.* (2011) in the special case are presented in Fig. 2. It is observed that our results in the limiting case ($Re = 0, \alpha = 0$) are

in close agreement with corresponding result of Srinivas *et al.* (2011). The solution of Srinivas *et al.* (2011) is analytical approximation computed by perturbation method.
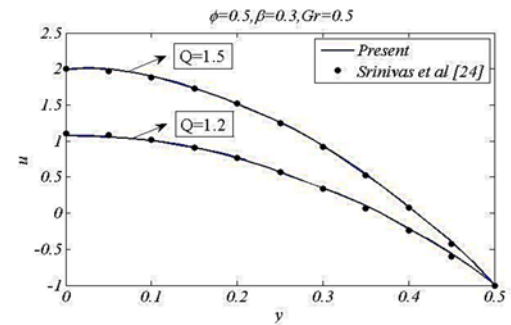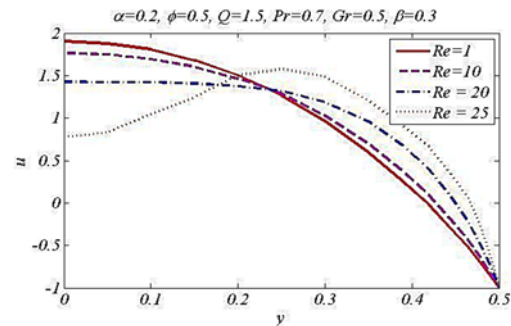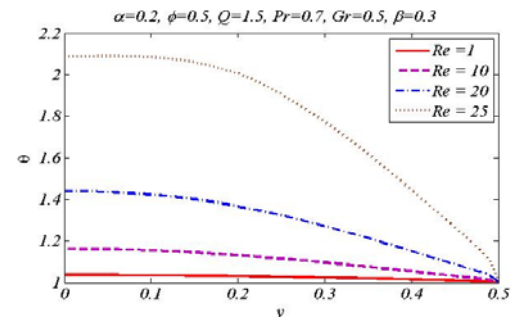

Fig. 2. Comparison of velocity profile for present results with Srinivas *et al.* (2011).
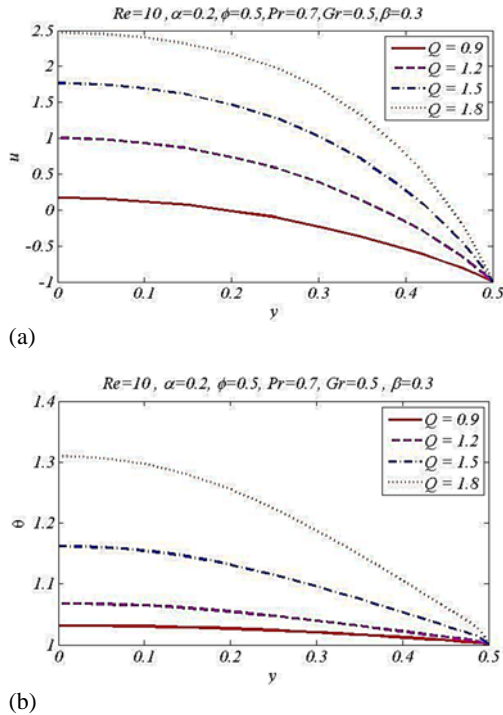

(a)

(b)

Fig. 3. (a) Longitudinal velocity distribution and (b) temperature profile for different values of Re when other parameters are fixed at $\alpha = 0.2$, $\varphi = 0.5, Q = 1.5, Pr = 0.7, Gr = 0.5, \beta = 0.3$.

The longitudinal velocity u and the temperature profile θ are presented in the Figs. 3 – 6 to see the effect of Reynolds number Re, time mean flow rate Q, Grashof number Gr and heat generation parameter β. From these figures, it is observed that both velocity and temperature achieve maximum in the vicinity of the center of the channel. Moreover, parabolic behavior by velocity and temperature graphs is observed in al cases. In Fig. 3(a), we observe the effect of Reynolds number Re on velocity distribution. We see that near the center of the channel, increase in Re causes a decrease in velocity while an opposite behavior is observed at the wall. So, it predicts that dominant inertial effects

to viscous forces in the center of the channel causes decrease in velocity of the fluid while in the region of the wall dominance of inertial forces enhances the velocity. Fig. 3(b) illustrates that an increase in Re rises the temperature over the whole cross-section. This observation is not reported in earlier studies and it attributed to strong inertial effects induced for large values of Reynolds number. Moreover, long wavelength and low Reynolds number theory is not able to predict such non-linear effect.

(a)

(b)

Fig. 4. (a) Longitudinal velocity distribution and (b) temperature profile for different values of Q when other parameters are fixed at $Re = 10, \alpha = 0.2, \varphi = 0.5, Pr = 0.7, Gr = 0.5, \beta = 0.3.$

Figures 4(a) and 4(b) show the effect of time mean flow rate Q on velocity distribution and temperature profile, respectively. Both figures show that the rise in volume flow rate Q enhances longitudinal velocity and temperature profile. Fig. 5(a) presents the effect of Grashof number Gr on longnitudanl velocity profile. We see that the behavior of velocity due to Grashof number Gr at the wall and near the center is different. In the region $0 \leq y \leq 0.2$, we observe that dominance of buoyancy forces reduces the velocity but after this region $y \geq 0.2$, increase in velocity is observed by same behavior of Gr. Fig. 5(b) exhibits the decreasing behavior in temperature distribution by enhancing Gr in the whole domain. As increase in Grashof number corresponds to enhance the buoyancy forces caused by temperature difference, which sufferers its effect in the center of the channel and so causes the decrease in rise in temperature. In Fig. 6(a), we observe that for the velocity distribution, heat generation parameter β exhibits same behavior as in case of Grashof number but in Fig. 6(b) temperature increases due to increase in the heat generation parameter β, which is quite

natural. Hence Grashof number Gr also helps to control the heat in the fluid flow with heat generation parameter and its effects are opposite to the effect of heat generation parameter β.
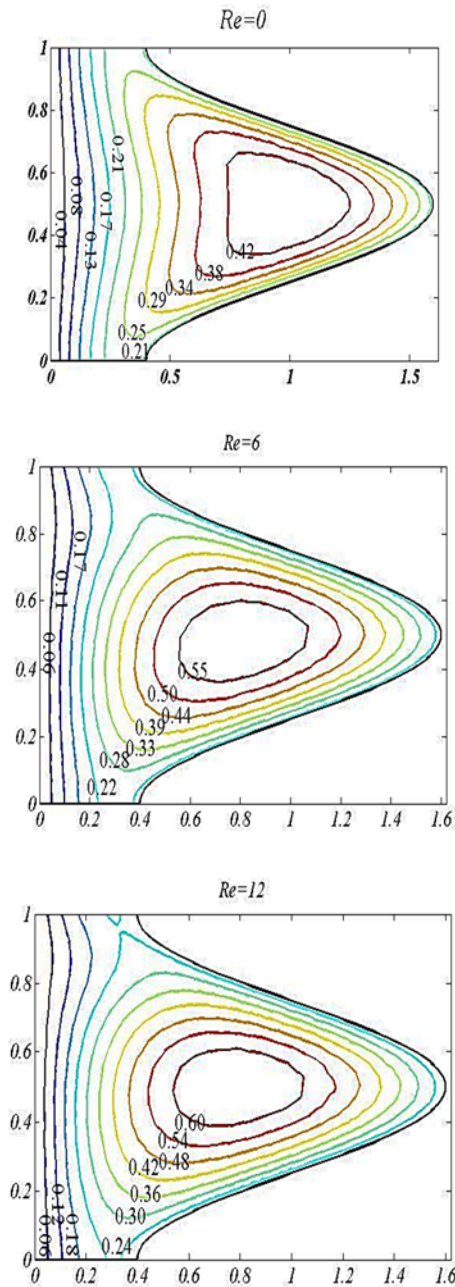

(a)

(b)
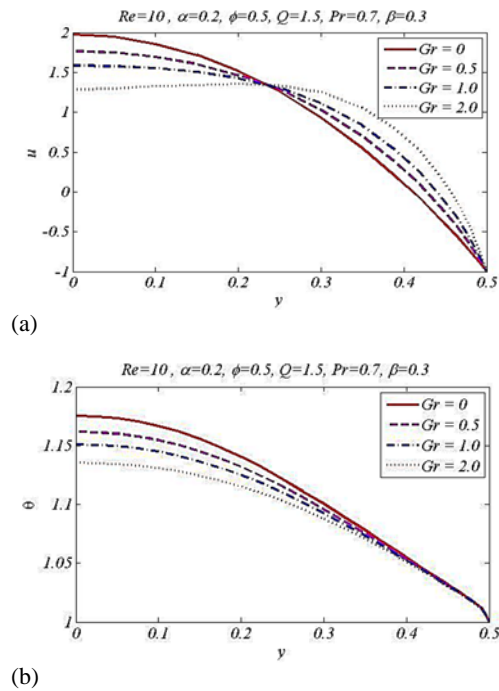
Fig. 5. (a) Longitudinal velocity distribution and (b) temperature profile for different values of Gr when other parameters are fixed at $Re = 10, \alpha = 0.2, \varphi = 0.5, Q = 1.5, Pr = 0.7, \beta = 0.3.$

(a)

(b)
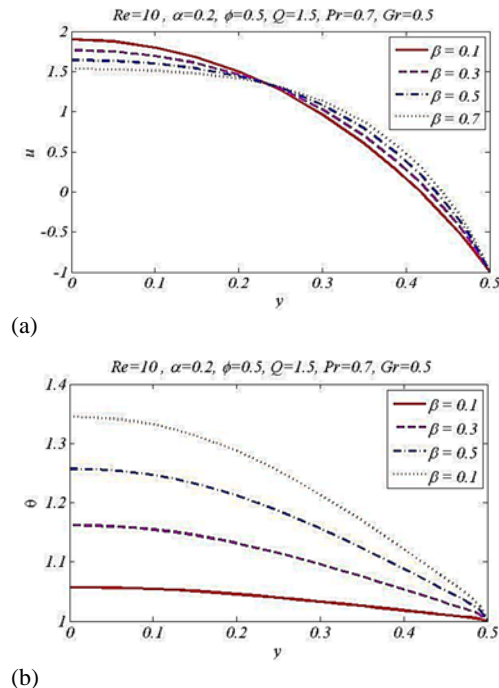
Fig. 6. (a) Longitudinal velocity distribution and (b) temperature profile for different values of β when other parameters are fixed at $Re = 10, \alpha = 0.2, \varphi = 0.5, Q = 1.5, Pr = 0.7, Gr = 0.5.$
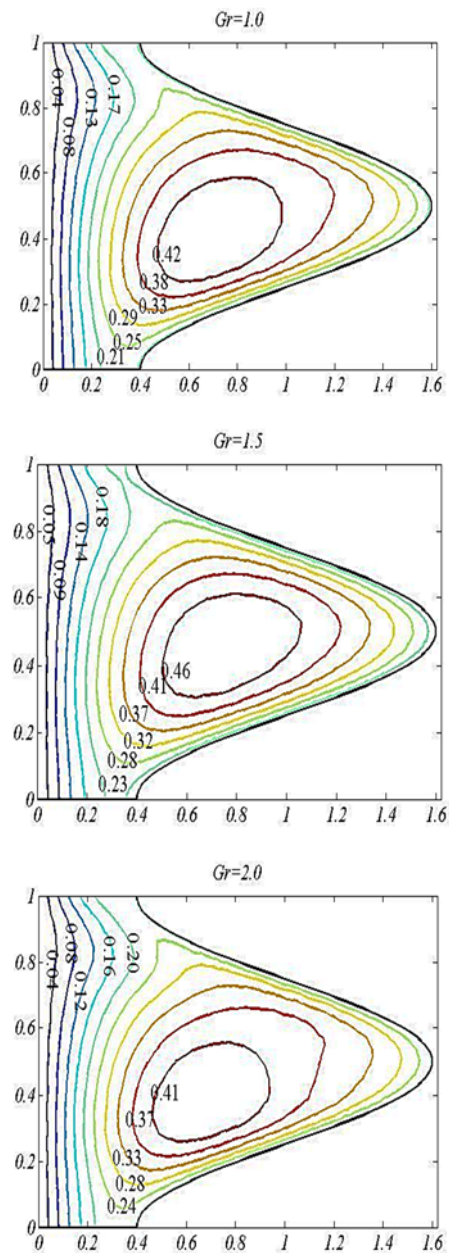
variation of Reynolds number Re. It is observed that size of bolus magnifies with the increase in Reynolds number and as far as the number of bolus are concern, we observe that number of boluses also increases with increase in Re. It is due to the fact that increase in inertial effects causes rise in velocity profile of the fluid so thesolution surface attains more height. Fig. 8 shows the variation of streamlines for different values of Grashof number Gr. It is noticed that the trapped bolus exits near the central region of the channel for smaller values of Grashof number. Moreover, it moves in lower region of the boundary wall with increase in Grashof number as shown in Fig. 8.
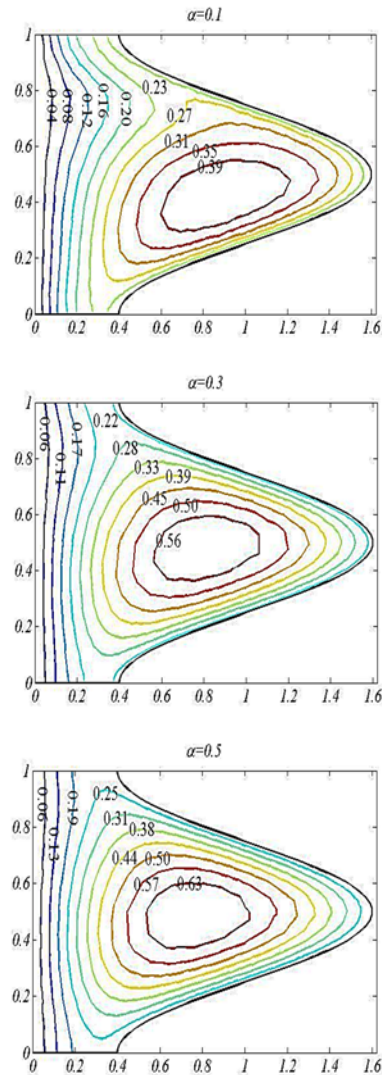
Fig. 7. Variation of streamlines in wave frame of reference for different values of Re with fixed values of $\alpha = 0.3, \phi = 0.6, Q = 1.2, Gr = 0.5, Pr = 0.7, \beta = 0.3.$

5.2 Trapping and Vorticity

The behavior of streamlines in wave frame for stationary wall is mostly similar as that of wall but sometime situation arises that pattern of streamlines can split and encloses a bolus of fluid particles in closed streamlines form so that circular region is created. On the other hand, in the fixed frame, the waves trapped the fluid bolus and traps it with speed of wave. To examine the variation of streamlines, we plotted contours of streamlines for different values of the parameter involved as shown in Figs. 7 – 11.

Figure 7 shows the behavior of streamlines with

Fig. 8. Variation of streamlines in wave frame of reference for different values of Gr with fixed values of $Re = 6, \alpha = 0.3, \phi = 0.6, Q = 1.2, Pr = 0.7, \beta = 0.3.$

Fig. 9. Variation of streamlines in wave frame of reference for different values of β with fixed values of $Re = 6, \alpha = 0.3, \phi = 0.6,$ $Q = 1.2, Gr = 0.5, Pr = 0.7.$

Figure 9 provides the behavior of heat generation parameter β. From this figure, we observe the increase in the size of bolus with increase in heat generation parameter β. Fig. 10 shows increase in the size of traped bolus with increase in wave number α. It is also observed that for small α, the bolus are trapped near the wall but when we increase the wave number α, the bolus moves to the central part of the region. Fig. 11 illustrates the effect of time mean flow rate Q on the streamlines. We observed a rapid increase in the number and size of bolus with small increase in the flow rate Q. In Figs. 12 – 17, we plotted the isothermal lines for different flow parameters. In Fig. 12, we have observed that by

increasing in Reynolds number, isothermal lines shows enhanced curvature effects and formation of bolus appears where complete bolus is developed in the central region for $Re = 12$. Fig. 13 shows that increase in Grashof number increases curvature effects near central wall and shows same smoothness of curvature near the peristaltic wall in all cases. Fig. 14 exhibits the effect of increasing heat generation parameter β on isothermal lines. It is observed that isothermal lines congregated at central wall and moves towards the wall channel. Variation in isothermal lines for different values of Prandtl number Pr may be seen in Fig. 15.
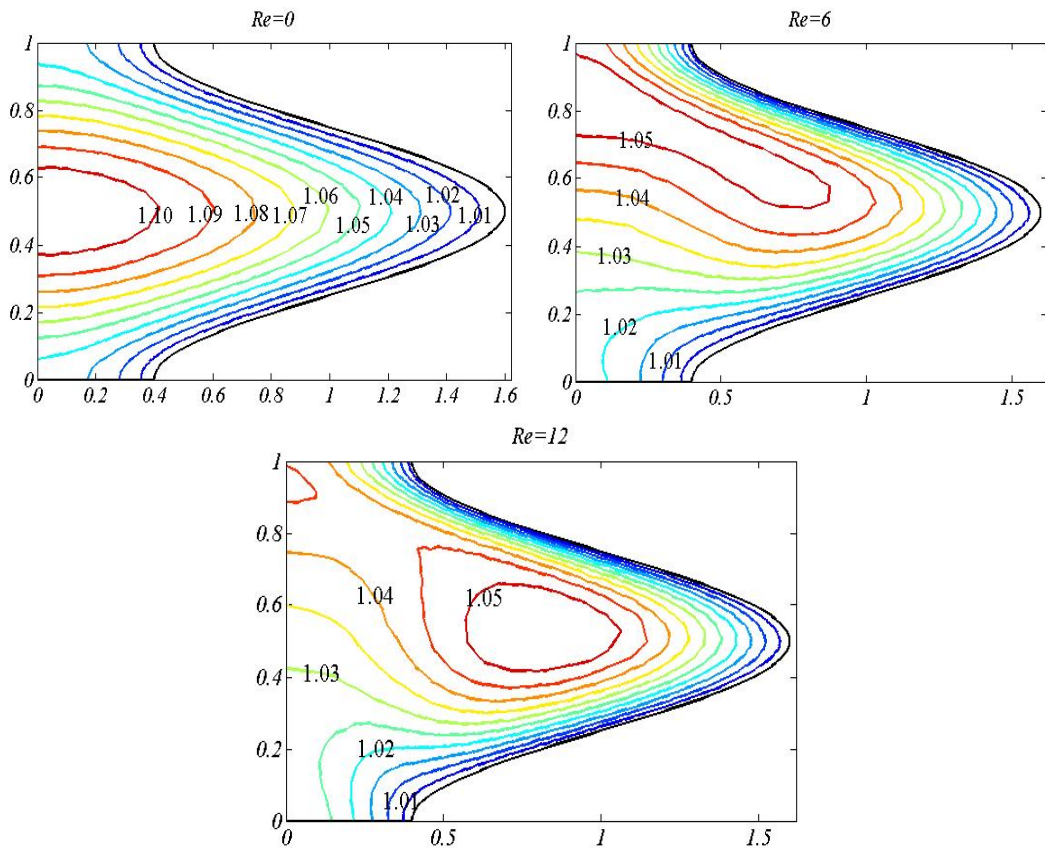

Fig. 10. Variation of streamlines in wave frame of reference for different values of α with fixed values of $Re = 6, \phi = 0.6, Q = 1.2,$ $Gr = 0.5, Pr = 0.7, \beta = 0.3.$

We can see that more curvature effect in central region with more number of bolus by increases the value of Pr. Fig. 16 shows decrease in curvature of isothermal lines with increase in the wave number α.
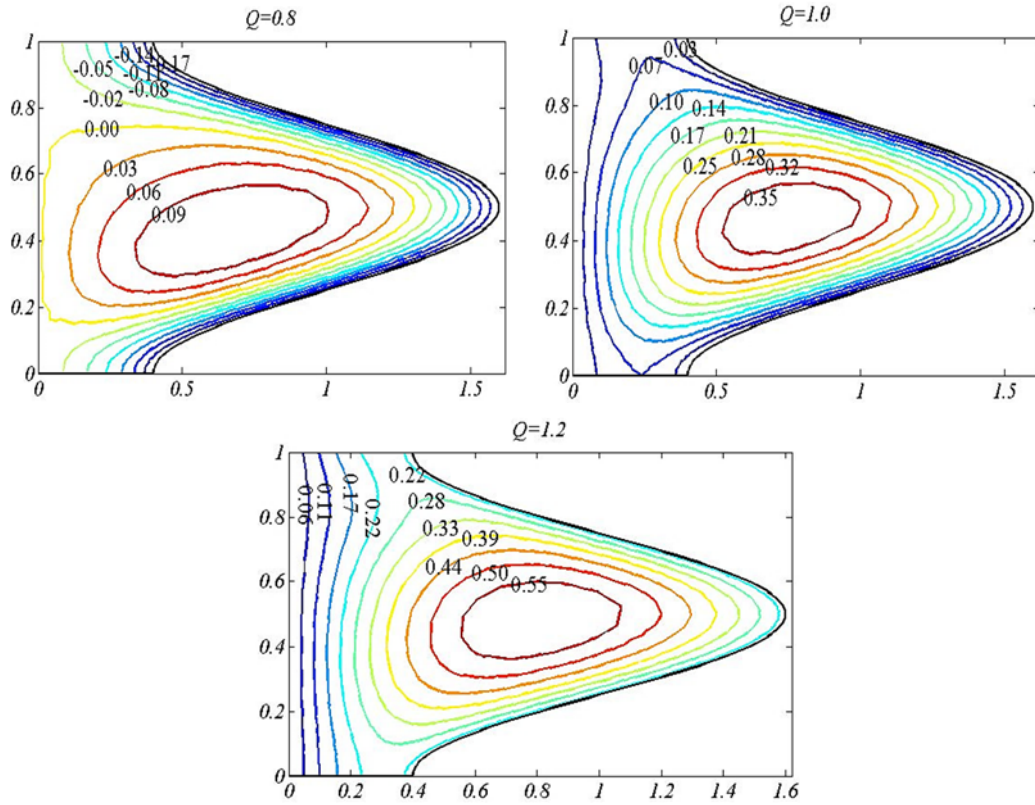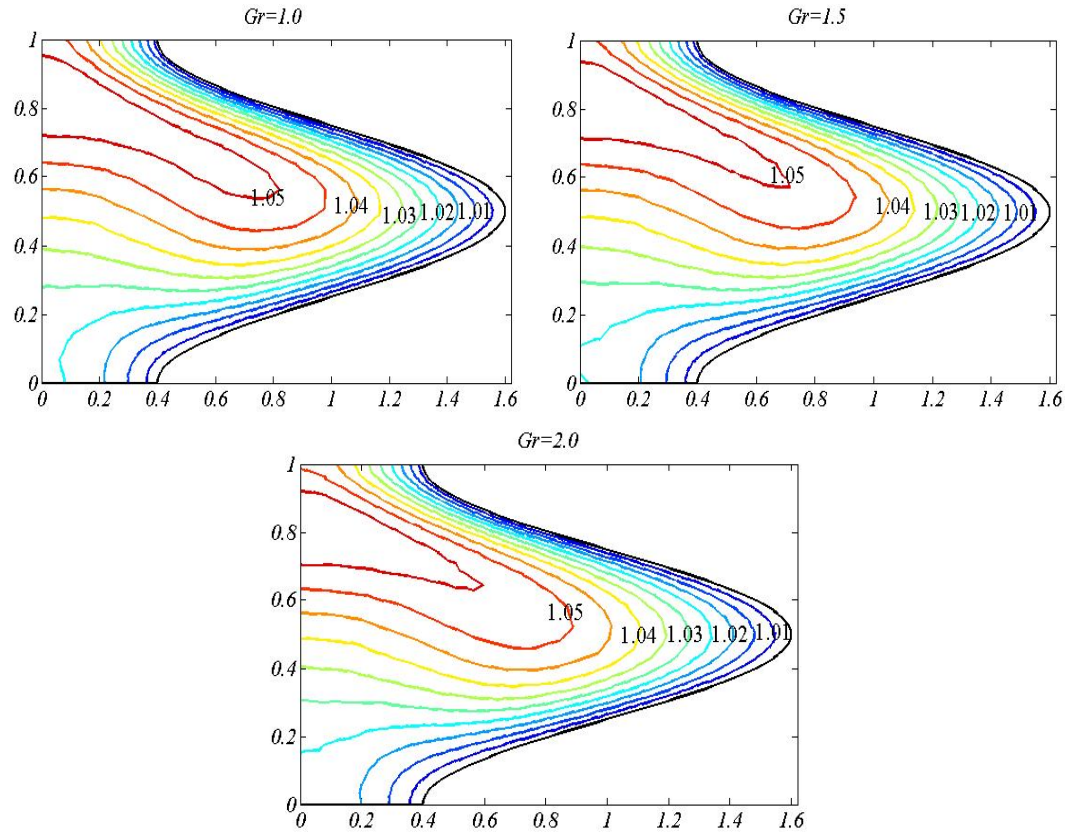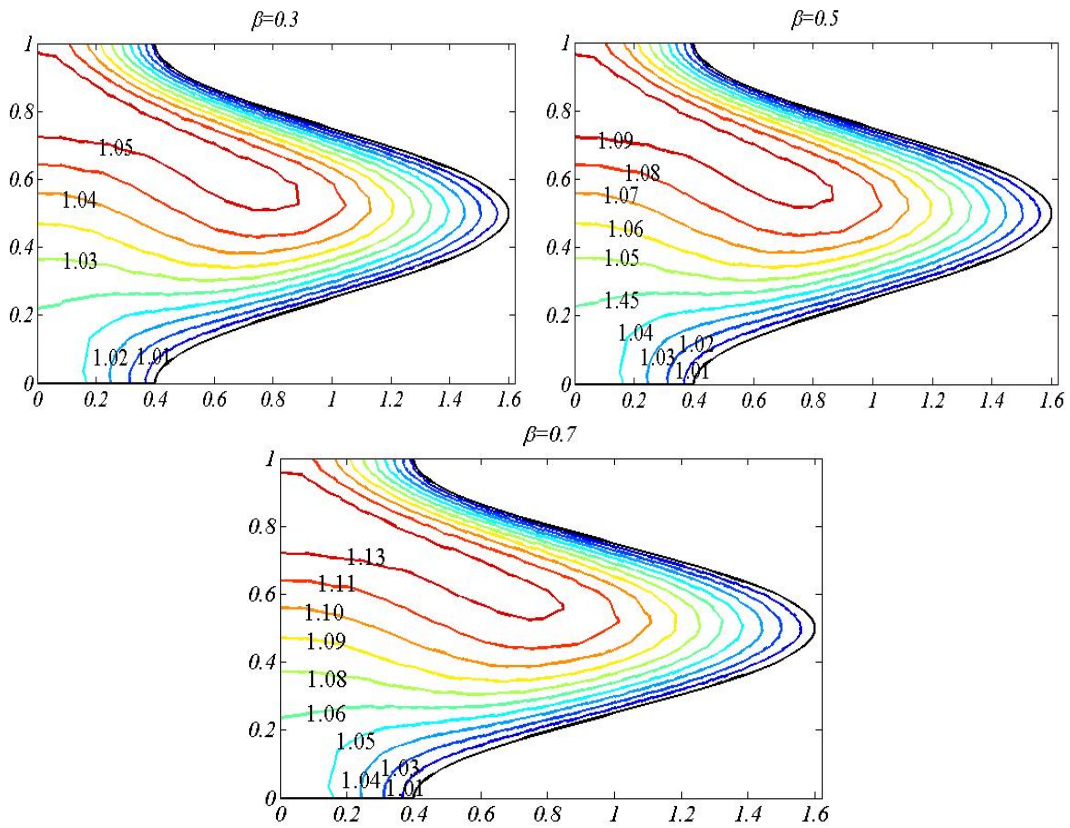
Fig. 11. Variation of streamlines in wave frame for different values of Q with fixed values of $Re = 6, \alpha = 0.3, \phi = 0.6, Gr = 0.5,$
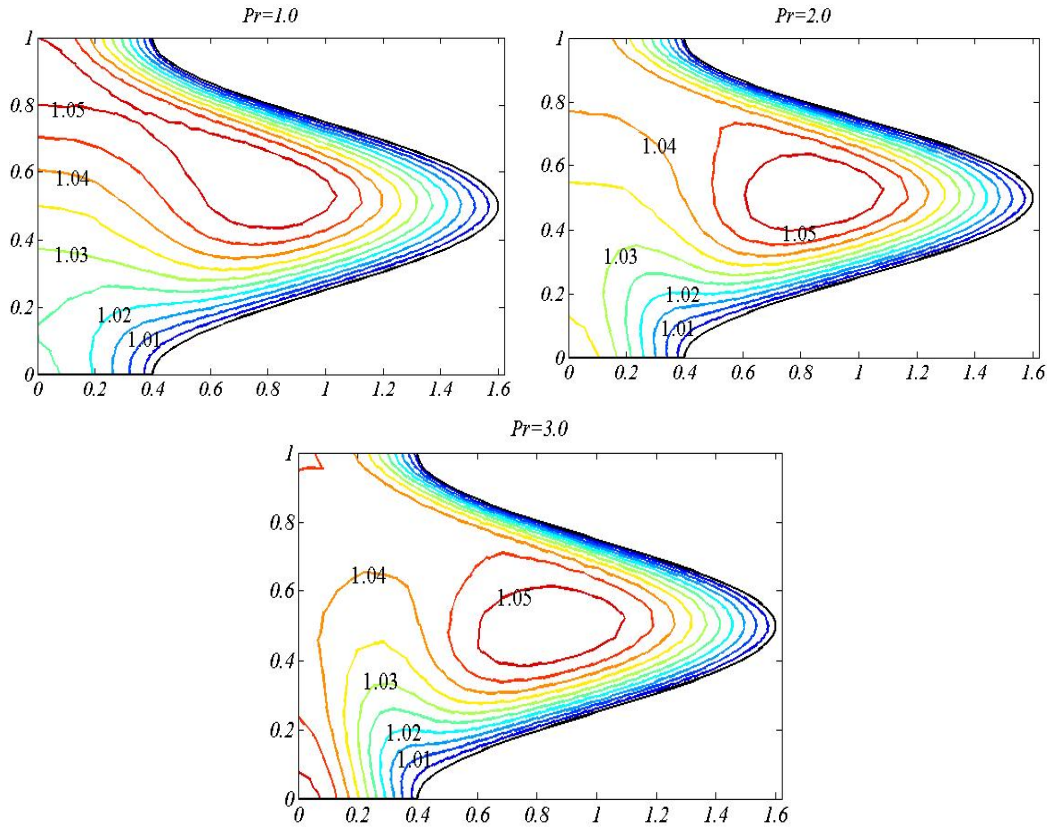**$Pr = 0.7, \beta = 0.3.$**

Fig. 12. Variation of Isothermal lines in wave frame of reference for different values of Re with fixed values of $\alpha = 0.3, \phi = 0.6, Q = 1.2, Gr = 0.5, Pr = 0.7, \beta = 0.3.$
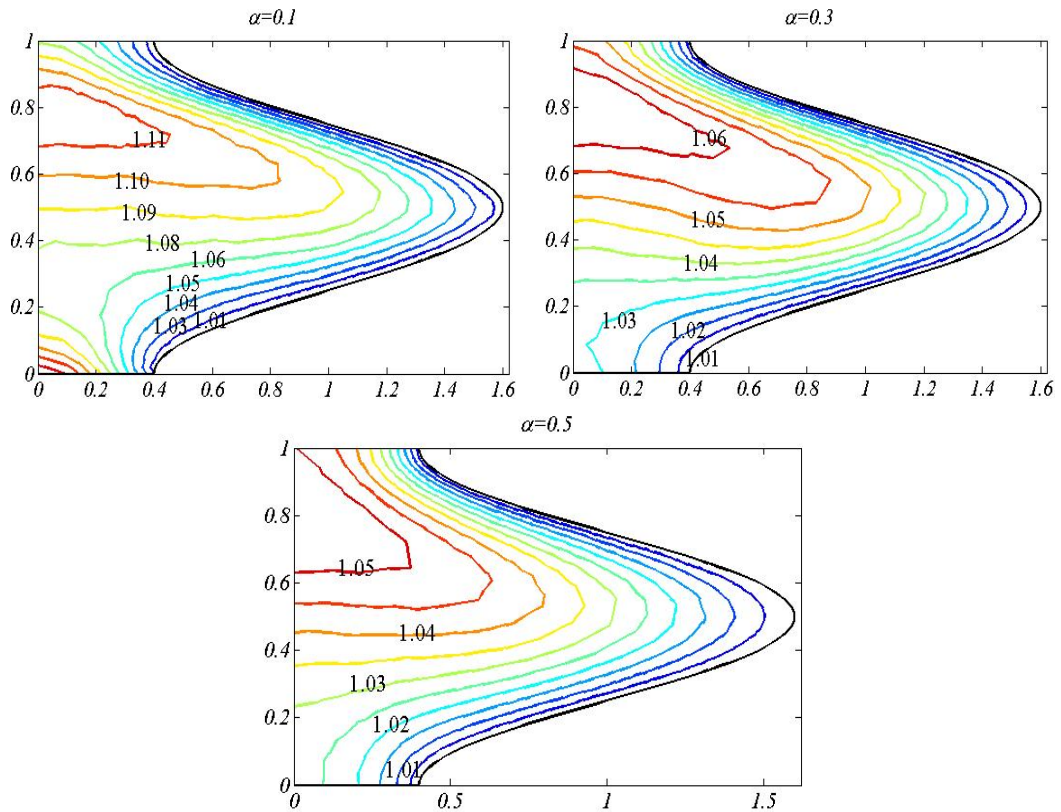
Fig. 13. Variation of Isothermal lines in wave frame of reference for different values of Gr with fixed values of $Re = 6, \alpha = 0.3, \phi = 0.6, \ Q = 1.2, Pr = 0.7, \beta = 0.3$.

Fig. 14. Variation of Isothermal lines in wave frame of reference for different values of β with fixed values of $Re = 6, \alpha = 0.3, \phi = 0.6, \ Q = 1.2, Gr = 0.5, Pr = 0.7$.
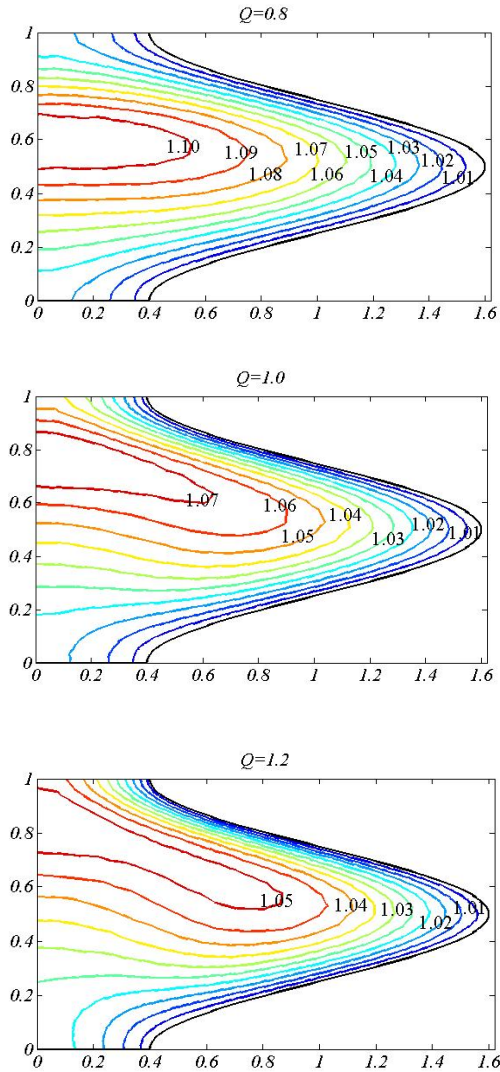
Fig. 15. Variation of Isothermal lines in wave frame of reference for different values of Pr with fixed values of $Re = 6, \alpha = 0.3, \phi = 0.6, \ Q = 1.2, Pr = 0.7, \beta = 0.3.$
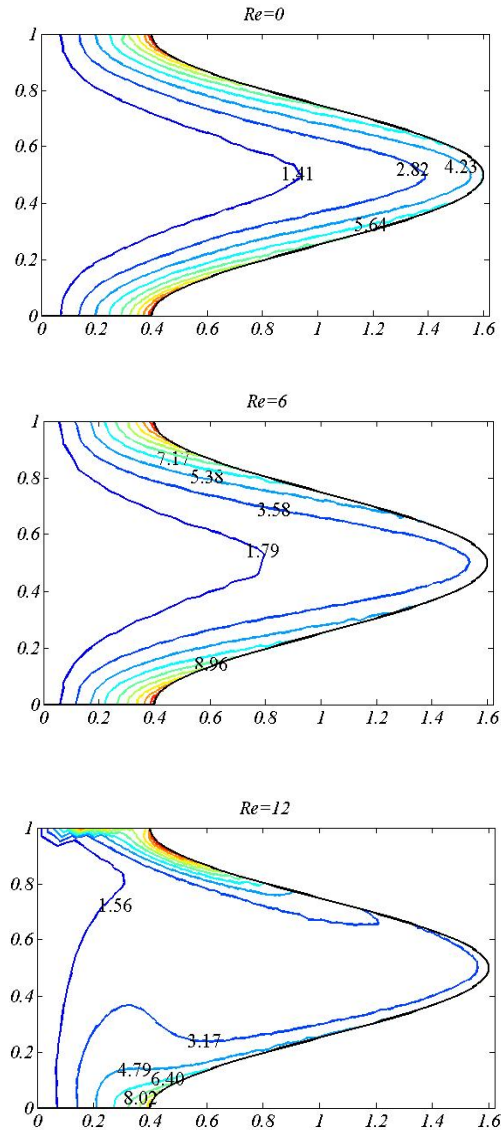

Fig. 16. Variation of Isothermal lines in wave frame of reference for different values of α with fixed values of $Re = 6, \phi = 0.6, Q = 1.2, Gr = 0.5, Pr = 0.7, \beta = 0.3.$

Fig. 17. Variation of Isothermal lines in wave frame of reference for different values of Q with fixed values of $Re = 6, \alpha = 0.3, \phi = 0.6, Gr = 0.5, Pr = 0.7, \beta = 0.3$.
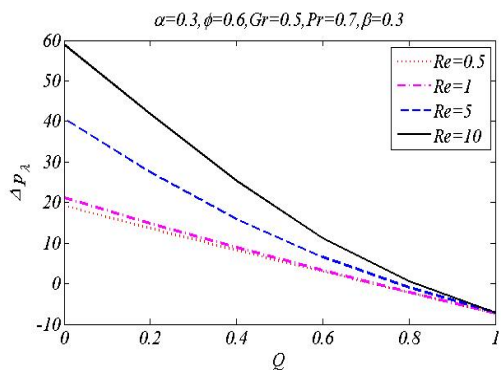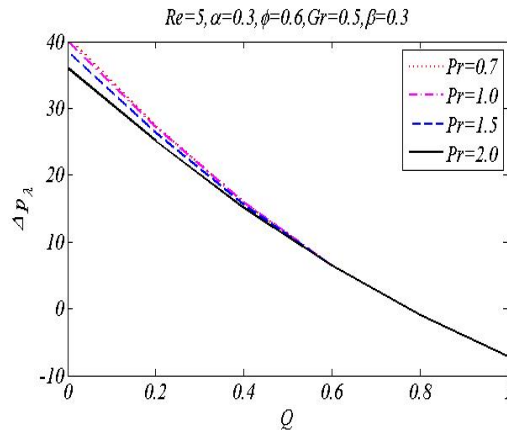
In Fig. 17, we see the effect of time mean flow rate Q on isothermal lines which exhibits that increase in this parameter causes the bending of isothermal lines in the central part of the channel towards upper region. The effect of Reynolds number Re on vorticity are presented in Fig. 18. It can be observed that vorticity is generated at the peristaltic wall and diffuses to the central region of the channel with increase in the values of Reynolds number.

5.3 Pressure Field Analysis

The pressure rise per wave length has been plotted in Figs. 19 – 24 against time mean flow rate for different range of values of involved parameters. There are following four types of flow region. When the flow is in regions $\Delta P_\lambda > 0$ and $Q > 0$ which means, in quadrant I then it is Peristaltic/Positive pumping.
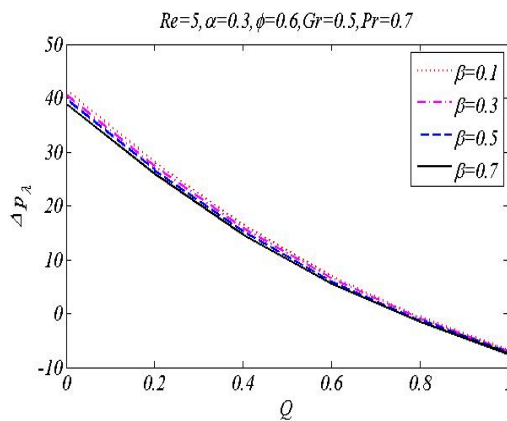

Fig. 18. Vorticity in wave frame of reference for different values of Re with fixed values of $\alpha = 0.3, \phi = 0.6, Q = 1.2, Gr = 0.5, Pr = 0.7, \beta = 0.3$.

Fig. 19. Pressure rise per wave length for varies value of Re.

Fig. 20: Pressure rise per wave length for varies value of Pr.
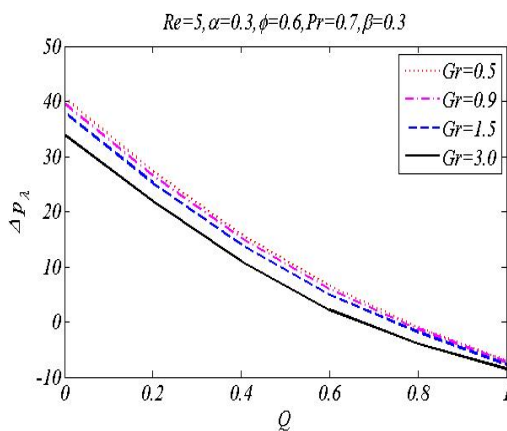
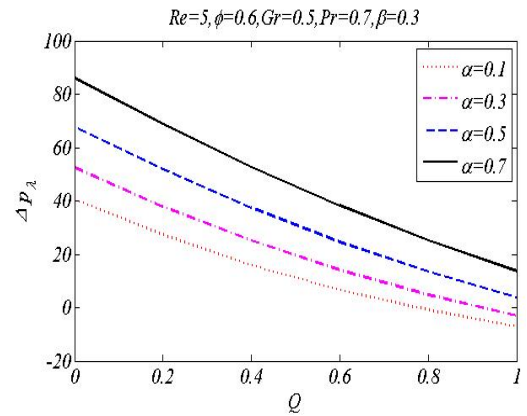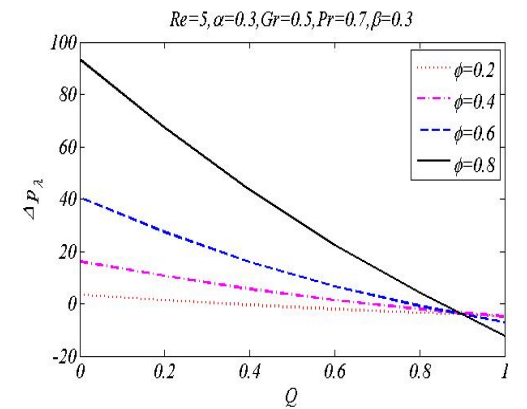**Fig. 21. Pressure rise per wave length for varies value of Gr.**

Fig. 22. Pressure rise per wave length for varies value of β.

When the flow is in regions $\Delta P_\lambda > 0$ and $Q < 0$ which means, in quadrant II then it is Retrograde/Backward pumping. When the flow is in regions $\Delta P_\lambda < 0$ and $Q < 0$ which means, in quadrant III then it is Co-pumping. When the flow is in regions $\Delta P_\lambda < 0$ and $Q < 0$ which means, in quadrant IV then it is augmented pumping. Also when the flow is in regions $\Delta P_\lambda = 0$ and $Q > 0$

which means, in quadrant IV then it is free pumping region. Pressure gradient is known as adverse pressure if $\Delta P_\lambda > 0$ and favorable pressure gradient if $\Delta P_\lambda < 0$. In Fig.(19), the effect of Reynolds number Re on pressure rise per wave length has been shown. We noticed that increase in Re causes increase in the pressure due to the dominance of inertial forces over viscous forces. It is due to the fact that when we increase Re, it enhances the inertial effect as compared to viscous effects, hence more pressure is required to maintain the flow in the channel. We further observed that when time mean flow rate approaches to 1, all the lines coincides which reflects the same amount of pressure at that point. It is observed from Figs. (20)–(22) that increase in Prandtl number Pr, Grashof number Gr and heat generation parameter β drops pressure rise per wave length but in the case of amplitude ratio ϕ and wave number α, opposite behavior is seen in Figs. (23) and (24) respectively.

Fig. 23. Pressure rise per wave length for varies value of α.

Fig. 24. Pressure rise per wave length for varies value of ϕ.

6. CONCLUSION

The heat and mass transfer analysis for peristaltic flow in a vertical channel has been presented. The governing equations are modelled in the absence of long wave length approximation which allows

us to observe the effect of all the parameter with moderate values. The numerical solutions for stream function, pressure rise per length as well as temperature profile are obtained. The effect of parameters on the velocity, heat transfer, and the trapping due to the peristaltic wall are discussed in detail. From the analysis the main outcomes for different flow characteristics are summarized. Increase in heat generation reduces the velocity near the central region and improves the velocity in neighbor of peristaltic wall. It also enhances the size of bolus and curvature effect on isothermal lines and drops the pressure. Increase in the Grashof number causes fall in velocity near the central region and rises the velocity neighbor of peristaltic wall and drops the pressure. Increase in time mean flow rate supports the enhancement of velocity, temperature and size of bolus. Increase in wave number increases size of bolus, reduces curvature effect of isotherms and rises the pressure.

REFERENCES

Ali N., M. Sajid, T. Javed and Z. Abbas (2010). Heat transfer analysis of peristaltic flow in a curved channel. *Int. J. Heat and Mass Transfer* 53, 3319-3325.

Dharmendra, T. and O. Anwer Beg (2013). Study of transient peristaltic heat flow through a finite porous channel. *Math. and Computer Modeling* **57**, 1270-1283.

Ekstein, E. C. (1970). Experimental and theoretical pressure studies of peristaltic pumping *SM. Thesis, Dept. Mech. Eng., Massachusetts Institute of Technology*, *Cambridge, MA*.

Fauci Lisa, J. (1992).Peristaltic pumping of solid particles. *Comp. Fluid* 21, 583-598.

Fung, Y. C. and C. S. Yih (1968). Peristaltic Transport. *J. of Appl. Mech.* 35 669-675.

Hamid, A. H., Tariq Javed, B. Ahmed and N. Ali. (2017). Numerical study of two-dimensional non-Newtonian peristaltic flow for long wavelength and moderate Reynolds number. *Brazilian Society of Mechanical Sciences and Engineering.*

Hayat, T., S. Farooq, A. Alsaedi and B. Ahmad (2017). Numerical study for Soret and Dufour effects on mixed convective peristalsis of Oldroyd 8-constants fluid. *International Journal of Thermal Sciences* 112, 68-81.

Hung, T. K. and T. D. Brown. (1975). Solid-Particle motion in two-dimensional peristaltic flows. *Journal of Fluid Mechanics* 73, 77-96.

Jaffrin, M. Y. (1973). Inertia and streamline Curvature Effects on Peristalsis. *International Journal of Engineering. Science* 11 681-699.

Latham T. W. (1966). Fluid motion in a peristaltic pump. *MIT, Massachusetts.*

Lew, H. S., Y. C. Fung and C. B. Lowenstein (1971). Peristaltic carrying and mixing of chyme in the small intestine. *Journal of Biomechanics* 4, 297-315.

Manton, M. J. (1975). Long-Wavelength Peristaltic pumping at low Reynolds number. *J.of Fluid Mech.* 68(3), 467-476

Mekheimer, Kh. S. (2008). Peristaltic flow of a magneto-micropolar fluid, Effect of induced magnetic field. *International J. of Appl. Mathematics.*

Narahari, M. and S. Sreenadh (2010). Peristalatic transport of a Bingham fluid in contact with a Newtonian fluid. *International J. of Applied Math. Mechanics* 6(11), 41–54

Ramesh, K. (2016). Effects of slip and convective conditions on the peristaltic flow of couple stress fluid in an asymmetric channel through porous medium. *Computer Methods and Programming in Biomedicne* 135, 1- 14.

Rao, A. R. and S. Usha (1995). Peristaltic transport of two immiscible viscous fluid in a circular tube. *J. of Fluid Mechanics* 85, 298–271.

Sajid, M., B. Ahmed and Z. Abbas (2015). Steady mixed convection stagnation point flow of MHD Oldroyd-B fluid over stretching sheet. *Journal of the Egyptian Mathematical Society* 23(2), 440-444.

Sayed, H. M., E. H. Aly and K. Vajravelu (2016). Influence of slip and convective boundary conditions on peristaltic transport of non-Newtonian Nano-fluids in an inclined asymmetric channel. *Alexandria Eng. J.* 55 (3) 2209-2220.

Shapiro, A. H. (1967). Pumping and retrograde diffusion in peristaltic waves. In Proc. *Workshop Ureteral Reftm Children*, *Nat. Acad. Sci*., *Washington, DC*, 1,109-126.

Shapiro, A. H. M. Y. Jaffrin and S. L. Weinberg (1969). Peristaltic Pumping with Long Wavelength at Low Reynolds Numbers. *Journal of Fluid Mechanics 37,* 799-825.

Shapiro, A. H., M. Y. Jaffrin and S. L. Weinberg (1969). Peristaltic Pumping with Long Wavelength at Low Reynolds Numbers. Journal of Fluid Mechanics 37, 799-825.

Srinivas, S. and M. Kothandapani (2008). Peristaltic transport in an asymmetric channel with heat transfer: A note, *International Communications in Heat and Mass Transfer* 35 (4), 514–522.

Srinivas, S., R. Gayathri and M. Kothandapani. (2011). Mixed convective heat and mass transfer in an asymmetric channel with peristalsis. *Comm. in Nonlinear Science and numerical simulation* 16, 1845-1862.

Sucharitha, G., P. Lakshminarayana and N. Sandeep. (2017). Joule heating and wall flexibility effects

on the peristaltic flow of magnetohydrodynamic nanofluid. *International Journal of Mechanical Sciences* 131, 52-62.

Takabatake, S., K. Ayukawa and M. Sawa (1989). Finite element Analysis of Two dimensional Peristaltic flow (1st Report, Finite element solution). *Japan Society of Mech. Eng.* 53, 1207-1213.

Tanveer, A., T. Hayat, A. Alsaedi and B. Ahmad. (2017). Mixed convective peristaltic flow of Sisko fluid in curved channel with homogeneous-heterogeneous reaction effects. *Journal of Molecular Liquids* 233 131-138.

Vajravelu, K., G. Radhakrishnamacharya and V. Radhakrishnamurty (2007). Peristaltic flow and heat transfer in a vertical porous annulus with longwave approx. *Inter. J. of Non-Linear Mech.* 42, 754 – 759.

Weinberg, S. L., E. C. Eckstein and A. H. Shapiro (1971). An experimental study of peristaltic pumping. *Journal of Fluid Mechanics* 49, 461-479.

Zein, T. F. and S. A. Ostrach (1970). A Long wavelength Approximation to Peristaltic Motion. *Journal of Biomech.* 3 63-75.